Acknowledgment. A Killam Postgraduate Scholarship (to Z.S.) from Dalhousie University and the financial assistance of the Natural Sciences and Engineering Research Council of Canada in the form of an Operating Grant (to R.J.B.) are gratefully acknowledged.

Appendix

In terms of the VB configurations[8]

$$\underset{\mathbf{1}}{N{:}^{-}R{\cdot\cdot}X}, \quad \underset{\mathbf{2}}{N{\cdot\cdot}RX{:}^{-}}, \quad \underset{\mathbf{3}}{N{:}^{-}R^{+}{:}X^{-}}, \quad \underset{\mathbf{4}}{N{\cdot}R{:}^{-}{\cdot}X},$$

$$\underset{\mathbf{5}}{N{:}^{-}R{:}^{-}X^{+}}, \quad \underset{\mathbf{6}}{N^{+}R{:}^{-}X{:}^{-}}$$

the TS wave function can be written as a linear contribution as follows:

$$\Psi_{TS} = c_1\psi_1 + c_2\psi_2 + c_3\psi_3 + c_4\psi_4 + c_5\psi_5 + c_6\psi_6$$

The reactant wave function can be written[29] as a linear combination of VB configurations which contain the nucleophile N^-

$$\Psi_r = a_1\psi_1 + a_2\psi_3 + a_3\psi_5$$

and the product wave function can be written as an equivalent linear combination of VB configurations involving the leaving group X^-

$$\Psi_p = b_1\psi_2 + b_2\psi_3 + b_3\psi_6$$

The contributions of ψ_5 and ψ_6 to Ψ_{TS} are small[8] and are relatively unimportant since they involve a two-electron transfer to form high-energy configurations. Hence

$$\Psi_{TS} \approx a\Psi_r + b\Psi_p + c\psi_3 + d\psi_4 + e\psi_1 + f\psi_2$$

Although, it is not possible to determine the values of the six coefficients (a, b, c, d, e, f) from the integrated charges, it is possible to estimate the upper bounds of a and b by the following approximations. Assuming $e = f = 0$, yields

$$\Psi_{TS} = a\Psi_r + b\Psi_p + c\psi_3 + d\psi_4$$

and applying the argument of Shaik[30] yields

$$Q_X = a^2Q_{X(\Psi_r)} + b^2Q_{X(\Psi_p)} + c^2Q_{X(\psi_3)} + d^2Q_{X(\psi_4)}$$

$$Q_N = a^2Q_{N(\Psi_r)} + b^2Q_{N(\Psi_p)} + c^2Q_{N(\psi_3)} + d^2Q_{N(\psi_4)}$$

$$Q_R = a^2Q_{R(\Psi_r)} + b^2Q_{R(\Psi_p)} + c^2Q_{R(\psi_3)} + d^2Q_{R(\psi_4)}$$

$$a^2 + b^2 + c^2 + d^2 = 1$$

where $Q_{X(\Psi_x)}$ is the charge on X obtained from wave function Ψ_x. Clearly, from the net charge on the reaction system

$$Q_X + Q_N + Q_R = -1$$

Furthermore, from the VB configurations we have

$$Q_{X(\Psi_p)} = Q_{N(\Psi_r)} = -1$$

$$Q_{X(\psi_4)} = Q_{N(\psi_4)} = 0$$

$$Q_{X(\psi_3)} = Q_{N(\psi_3)} = -1$$

$$Q_{R(\psi_3)} = 1, \quad Q_{R(\psi_4)} = -1$$

$$Q_{X(\Psi_r)} = -Q_{R(\Psi_r)}$$

$$Q_{N(\Psi_p)} = -Q_{R(\Psi_p)}$$

This leads to the following three equations

$$Q_X = a^2Q_{X(\Psi_r)} - b^2 - c^2$$

$$Q_N = b^2Q_{N(\Psi_p)} - a^2 - c^2$$

$$Q_R = a^2Q_{R(\Psi_r)} + b^2Q_{R(\Psi_p)} + c^2 - d^2$$

We can obtain Q_X, Q_N, Q_R, $Q_{X(\Psi_r)}$, and $Q_{N(\Psi_p)}$ by integrating the electron density over the corresponding basin with the corresponding wave function, and finally by setting c^2 or $d^2 = 0$, we can evaluate a^2, b^2 and d^2 or c^2. In each case the choice between $c^2 = 0$ or $d^2 = 0$ is made on the basis that only one of these two possibilities yields plausible values. For example, if c^2 is set equal to zero for N = X = H, then $a^2 = b^2 = 0.60$. Clearly, $a^2 + b^2 > 1$ is unreasonable, and therefore we chose the solution given in Table II ($a^2 = b^2 = 0.40$ and $c^2 = 0.20$).

Registry No. H, 12184-88-2; CH_4, 74-82-8; HO, 14280-30-9; F, 16984-48-8; Cl, 16887-00-6; CH_3F, 593-53-3; CH_3Cl, 74-87-3; CH_4O, 67-56-1.

(29) Harcourt, R. D. THEOCHEM **1988**, *165*, 329.

(30) Reference 8, page 285.

Degenerate and Pseudodegenerate 1,3-Nitrogen Shifts in Sulfur–Nitrogen Chemistry: ^{15}N NMR Analysis of Skeletal Scrambling in $PhCN_5S_3$

Ketut T. Bestari, René T. Boeré, and Richard T. Oakley*

Contribution from the Guelph Waterloo Centre for Graduate Work in Chemistry, Department of Chemistry and Biochemistry, University of Guelph, Guelph, Ontario, N1G 2W1, Canada.
Received March 22, 1988

Abstract: Skeletal scrambling in the 1,3-NSN-bridged 5-phenyl-1,3,2,4,6-dithiatriazine ($PhCN_5S_3$) has been studied by NMR analysis of the exchange of ^{15}N-labeled nitrogen between different sites. A mechanism involving two simultaneous 1,3-nitrogen shift pathways, via carbon and sulfur, is proposed, and is supported by correlation of the observed depletion/enrichment rates with those predicted by a model based on two sets of coupled first-order site exchanges. Eyring analysis of the temperature dependence of the two first-order rate constants k_c and k_s affords activation parameters $\Delta H^{\ddagger} = 19$ (±1) kcal mol^{-1} and $\Delta S^{\ddagger} = 1$ (±5) cal mol^{-1} K^{-1} (for the carbon pathway) and $\Delta H^{\ddagger} = 22$ (±1) kcal mol^{-1} and $\Delta S^{\ddagger} = 6$ (±5) cal mol^{-1} K^{-1} (for the sulfur pathway). The barriers to both skeletal scrambling in and thermal decomposition of $PhCN_5S_3$ and related heterocycles are discussed in terms of their electronic structures.

Our understanding of the structures of molecules containing conjugated –S=N– units is based on extensive crystallographic evidence; the use of spectroscopic methods for structural analysis has been limited by the absence of convenient NMR probes. In the last decade, however, advances in both synthetic and instrumentational techniques have allowed the development of both ^{14}N

0002-7863/89/1511-1579$01.50/0

Scheme I

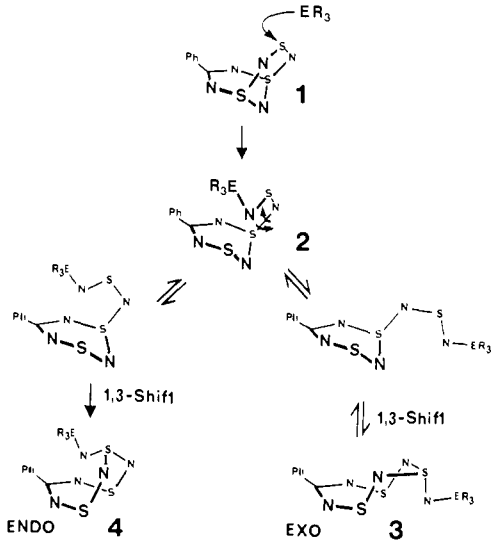

Scheme II

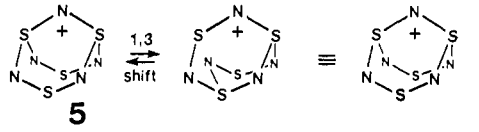

and ^{15}N NMR spectroscopy[1-4] as effective probes of molecular structure. Indeed, we have recently demonstrated the use of ^{15}N NMR for the characterization of reaction intermediates, i.e., during the conversion of the bicyclic derivative **1**, upon treatment with arsines and phosphines R_3E (E = As, P), into the *exo*- and *endo*-trithiatetrazocines **3** and **4** (Scheme I).[5] ^{15}N NMR analysis of this reaction established the intermediacy of the dithiatriazine **2**, which facilitates the isomerization of **3** into **4** by a series of 1,3-nitrogen shift steps.

The 1,3-nitrogen shift sequence which converts **3** into **4** effects a structural change (a configurational inversion); i.e., the rearrangement is nondegenerate. Degenerate 1,3-nitrogen shift reactions should also be possible; indeed, in 1980 Bartetzko and Gleiter suggested that such a process might lead to fluxional behavior in the $S_4N_5^+$ cation **5** (Scheme II.)[6] While observation and analysis of such scrambling, for example, by labeling methods, are possible in principle, it is not a simple task from an experimental point of view.[7] If, however, the structure of **5** is modified by replacing a (charged) sulfur atom with an isoelectronic PhC moiety, as in **1**, the pseudo-degenerate 1,3-nitrogen shift can be easily probed. Indeed, a preliminary NMR analysis of **1** specifically enriched with ^{15}N has shown that skeletal scrambling does occur.[8]

In the present paper we provide a detailed kinetic analysis of the isotopic exchange process in **1** and discuss the results in terms of the proposed 1,3-shift mechanism. The barriers to both skeletal scrambling in, and thermal decomposition of, heterocycles related to **1** are analyzed in terms of their electronic structures.

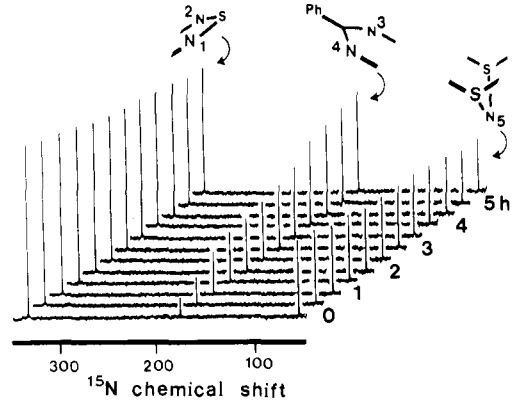

Figure 1. Time dependence of the ^{15}N NMR spectrum of **1** (in $CDCl_3$ with 0.05 M $Cr(acac)_3$) at 20 °C. The starting material was 99% enriched in ^{15}N at the N1,2 and N5 positions.

Scheme III

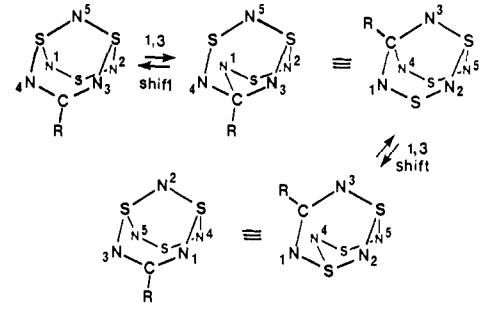

Scheme IV

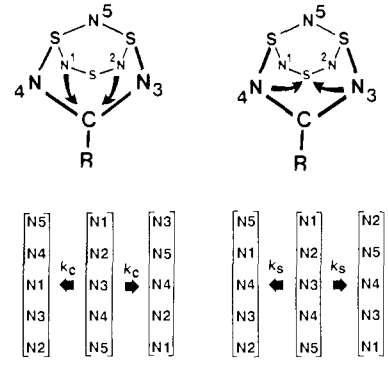

Results and Discussion

Pseudodegenerate Scrambling in 1. The observation of scrambling in **1** requires the introduction of ^{15}N labels at specific sites. Such material, with labels at the N1,2 and N5 sites, can be generated by treating *N,N,N'*-tris(trimethylsilyl)benzamidine with 99% ^{15}N-enriched $S_3N_3Cl_3$ at 0 °C in acetonitrile (eq 1).[8] The

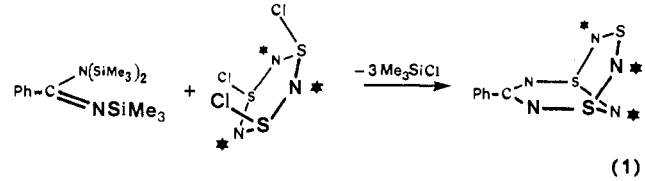

(1)

^{15}N NMR spectrum of the product, when freshly dissolved in chloroform, illustrates the two expected signals at δ 330.1 (N1,2) and 54.9 (N5) (Figure 1).

When a solution of this labeled material is left to stand at or near room temperature for several hours, a third signal at δ 176.1, corresponding to ^{15}N incorporation at the N3,4 positions, slowly grows in at the expense of the others (Figure 1). This exchange of the ^{14}N and ^{15}N nuclei can, at first sight, be rationalized in terms of two consecutive 1,3-nitrogen shifts similar to that shown

(1) Passmore, J.; Schriver, M. J. *Inorg. Chem.* **1988**, *27*, 2749.
(2) Chivers, T.; Oakley, R. T.; Scherer, O. J.; Wolmershäuser, G. *Inorg. Chem.* **1981**, *20*, 914.
(3) Burford, N.; Chivers, T.; Cordes, A. W.; Laidlaw, W. G.; Noble, M. C.; Oakley, R. T.; Swepston, P. N. *J. Am. Chem. Soc.* **1982**, *104*, 1282.
(4) Chivers, T.; Cordes, A. W.; Oakley, R. T.; Pennington, W. T. *Inorg. Chem.* **1983**, *22*, 2429.
(5) Boerē, R. T.; Cordes, A. W.; Oakley, R. T. *J. Am. Chem. Soc.* **1987**, *109*, 7781.
(6) Bartetzko, R.; Gleiter, R. *Chem. Ber.* **1980**, *113*, 1138.
(7) Salts of the $S_4N_5^+$ cation are heat, shock, and moisture sensitive, have limited solubility in many organic solvents and attack paramagnetic relaxation reagents (PARRs) such as $Cr(acac)_3$.
(8) Boerē, R. T.; Oakley, R. T.; Shevalier, M. *J. Chem. Soc., Chem. Commun.* **1987**, 111.

Table I. Rate Constants k_c and k_s

T (K)	k_c (10^{-6} s^{-1})	ρ	k_s (10^{-6} s^{-1})	ρ
278	2.70	0.997	0.319	0.988
283	5.30	0.996	0.706	0.991
288	9.65	0.999	1.54	0.998
293	16.3	0.997	2.79	0.998
298	30.2	0.994	5.01	0.990
303	52.3	0.996	9.13	0.991

Table II. Eyring Analysis of Rate Constant Data

pathway	$\Delta H^{\ddagger}$ (kcal mol^{-1})	$\Delta S^{\ddagger}$ (cal mol^{-1} K^{-1})	ρ
carbon	19 (±1)	1 (±5)	0.999
sulfur	22 (±1)	6 (±5)	0.999

in Scheme II for $S_4N_5^+$. Scheme III illustrates the two steps and also the redistribution of sites that this sequence affords.

The 1,3-shift described above is not unique. In addition to this pathway, hereafter referred to as the "carbon" pathway and characterized by a first-order rate constant k_c, there is a second 1,3-shift sequence, involving a single step via sulfur, that must also be considered. This latter process, the "sulfur" pathway, with first-order rate constant k_s, does not lead to ^{15}N scrambling between the initially labeled and unlabeled sites, but does effect a redistribution of ^{15}N between the N1,2 and N5 positions. The overall rate law predicted by the 1,3-nitrogen shift mechanism must accommodate both exchange routes, i.e., a superposition of the rate expressions arising from the coupled first-order site exchanges summarized in Scheme IV.

Kinetic Analysis. Analysis of the observed changes in ^{15}N enrichment in terms of the above mechanism required the development of a set of rate expressions for N1–N5 in terms of the eigenvalue procedure laid down by Matsen and Franklin.[9] Accordingly, we sought eigenintensities Qi (i = 1 to 5), linearly independent combinations of the ^{15}N intensities at Ni (i = 1 to 5), whose variation with time followed simple first-order kinetics. The algebraic solution of the eigenvalue problem afforded five eigenvalues, each expressed in terms of k_c and k_s (see Appendix). Three of these corresponded to eigenintensities which were invariant with time.[10] The remaining two eigenvalues λ_1 and λ_2 provided direct access to the first-order rate constants k_c and k_s.

Given numerical values for k_c and k_s, specific eigenintensities $Q1$ and $Q2$ and eigenvalues λ_1 and λ_2 could be easily evaluated. In the absence of this information, however, an infinite number of eigenintensities can be generated which depend only on the ratio k_c/k_s. Treatment of experimental data therefore required (i) an initial arbitrary choice of the k_c/k_s ratio (typically k_c/k_s = 1), (ii) generation of the two corresponding eigenintensities $Q1$ and $Q2$ by solving the secular determinant, (iii) linear regression analysis of the $Q1$ and $Q2$ functions expressed in terms of the experimental ^{15}N NMR intensities (see Experimental Section), (iv) extraction of the values of λ_1 and λ_2 from the slopes of first-order plots involving $Q1$ and $Q2$ and, finally, (v) calculation of a first set of values for k_c and k_s. These new values were in turn cycled through the secular determinant to provide improved eigenintensities, from which were generated new values of λ_1, λ_2, and hence k_c and k_s. This process was repeated until self-consistency was achieved; i.e., the derived values of k_c and k_s were unchanged from the input values. Final values for the rate constants k_c and k_s, along with the correlation coefficients (ρ) for the fit of the associated eigenintensities, are given in Table I. The close match between the predicted and experimental rate laws, as indicated by the simultaneous fit of the data to both $Q1$ and $Q2$, provides convincing evidence in support of the proposed dual pathway 1,3-nitrogen shift mechanism.

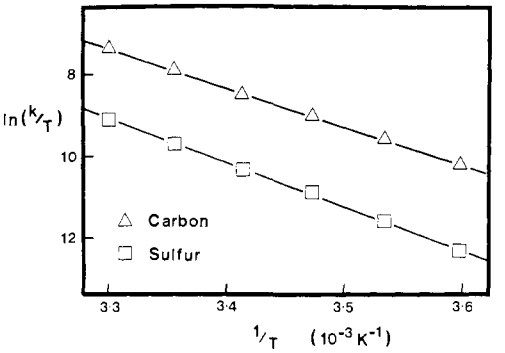

Figure 2. Eyring plot of rate constants for carbon and sulfur 1,3-shift pathways in **1**.

Scheme V

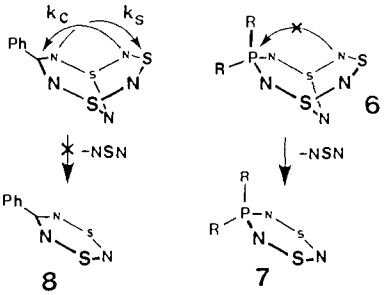

A study of the temperature dependence of the scrambling process was carried out over the temperature range 5–30 °C. Kinetic measurements outside this range were prohibited by the speed (slow or fast) of attainment of equilibrium. Eyring analysis of the rate constants k_c and k_s (Figure 2) afforded nearly identical activation parameters for the two pathways (Table II); $\Delta H^{\ddagger}$ = 19 (±1) kcal mol^{-1} and $\Delta S^{\ddagger}$ = 1 (±5) cal mol^{-1} K^{-1} (for the carbon pathway) and $\Delta H^{\ddagger}$ = 22 (±1) kcal mol^{-1} and $\Delta S^{\ddagger}$ = 6 (±5) cal mol^{-1} K^{-1} for the sulfur pathway. The small entropies of activation are consistent with an intramolecular process. The enthalpies of activation for these pseudodegenerate 1,3-nitrogen shifts are larger than those of the corresponding nondegenerate processes, e.g., in the conversion of **2** to **3** and **4**, where the exothermicity of the reactions presumably facilitates the transformation.[5]

Pseudodegenerate 1,3-Nitrogen Shifts in Related Structures. There are other structures, related to **1**, which could, in principle, undergo skeletal scrambling similar to that described above. For example, replacement of a (charged) sulfur atom in $S_4N_5^+$ (**5**) by a Ph_2P group instead of PhC affords the heterocycle **6** (Scheme V). Like **1**, **6** can be labeled in a fashion identical with that depicted in eq 1, i.e., by treatment of $Ph_2P(NSiMe_3)N(SiMe_3)_2$ with 99% ^{15}N labeled $S_3N_3Cl_3$.[8,11] However, we have been unable to observe any ^{15}N exchange at room temperature in this material. Attempts to force skeletal scrambling by heating samples of **6** at reflux in acetonitrile effect thermal decomposition into the phosphadithiatriazine **7**, a reaction shown previously to proceed with an Arrhenius activation energy of 25 kcal mol^{-1}.[12] The ^{15}N NMR spectrum of **7** shows virtually no incorporation of ^{15}N in the phosphorus-bound positions;[13] i.e., thermal loss of N1,2 from **6** is significantly faster than a 1,3-nitrogen shift involving phosphorus.

Electronic Considerations. A central theme in the study of the molecular systems composed from conjugated –S=N– linkages is the understanding of the relationships between electronic structure and structural stability.[14] In the case of molecules of

(9) (a) Matsen, F. A.; Franklin, J. L. *J. Am. Chem. Soc.* **1950**, *72*, 3337. (b) Szabó, Z. G. *Chemical Kinetics*; Ed. Bamford, C. H., Tipper, C. F. H., Eds.; Elsevier: 1969, Vol. 2, Chapter 1, pp 1–80.

(10) The mathematics is very similar to that involved in constructing the Hückel molecular orbitals of a five-orbital ring, starting from two separated three-orbital and two-orbital fragments. The totally symmetric combination, and the two a_2 symmetry eigenvectors, correspond to the three time-independent eigenintensities of the present problem.

(11) Chivers, T.; Dhathathreyan, K. S.; Liblong, S. W.; Parks, T. *Inorg. Chem.* **1988**, *27*, 1305.

(12) Burford, N.; Chivers, T.; Oakley, R. T.; Oswald, T. *Can. J. Chem.* **1984**, *62*, 712.

(13) The ^{15}N NMR signal for the phosphorus-bound nitrogens is expected at δ = 116.2 (see ref 3).

Table III. MNDO Charges and Bond Orders for EN_5S_3 Structures[a]

	E = S^+	E = CH	E = PH_2
	Charges		
E	1.108	0.227	0.615
N_a	−0.688	−0.533	−0.683
N_b	−0.688	−0.658	−0.682
S_a	1.180	0.951	0.973
S_b	1.108	0.903	0.896
N_c	−0.826	−0.795	−0.805
	Bond Orders		
E–N	1.438	1.429	0.980
N_a–S_a	0.914	0.992	1.065
S_a–N_b	0.914	0.858	0.829
N_b–S_b	1.438	1.435	1.437
S_a–N_c	1.022	1.009	0.993

[a] See Scheme VI for atom labeling.

Scheme VI

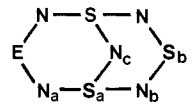

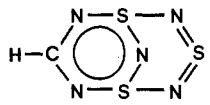

9

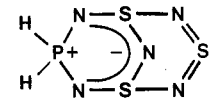

10

the type EN_5S_3 (E = S^+, S^-, R_2P, O_2S^-, RC), there are now two recognized pathways for structural change: the 1,3-shift mechanism reported here for E = RC (and proposed for S^+)[6] and the NSN-elimination reaction (thermal decomposition) known for E = R_2P, SO_2^-, and S^-.[8,12,15] The electronic factors that might influence the relative rates of these two processes deserve some comment.

Attempts to model the energetics of the 1,3-shift steps in **1**, **5**, and **6** have been unsuccessful; semiempirical molecular orbital codes such as MNDO do not provide an adequate simulation of the transition states. Some insight into the origin of the activation barriers, depicted qualitatively in Figure 3, can, however, be extracted from the variations in calculated (MNDO) charges and bond orders in several model EN_5S_3 structures (E = S^+, CH, and PH_2). Pertinent data are compiled in Table III. The largest, and most chemically significant, changes are in the N_a–S_a and S_a–N_b bond orders (see Scheme VI). Replacement of S^+ in $S_4N_5^+$ by a CH unit causes a strengthening of the N_a–S_a bonds at the expense of the S_a–N_b; i.e., the symmetric electron distribution found in $S_4N_5^+$ slides into a form reminiscent of the resonance representation **9**. The observed structural parameters in **1** certainly reflect this finding.[16] The slippage continues in $H_2PN_5S_3$; indeed, both the displacement of charge away from phosphorus and the bond order trends are suggestive of the internal salt formulation **10**.

If one assumes that an important energetic component of a 1,3-shift stems from the initial cleavage of the migrating S–N bond, then the N_a–S_a and S_a–N_b bond orders should be relatable to the observed activation parameters for the different 1,3-shift pathways. Accordingly, the strengths of the N_a–S_a and S_a–N_b bonds in RCN_5S_3 molecules can be correlated with the observation that migration of the N_a–S_a bond, i.e., the NC(R)N unit (Figure 3B), involves a greater activation energy than migration of the S_a–N_b bond, i.e., the NSN group (Figure 3A), this in spite of the fact that the latter pathway involves the generation of an intermediate structure with a four-coordinate carbon.[17] In $S_4N_5^+$ itself only a single pathway, involving migration of an NSN bridge between two sulfurs, is possible. We anticipate, based on the low N_a–S_a bond order and the absence of an intermediate structure, that the skeletal exchange in this system should be faster than either of the two pathways observed for RCN_5S_3 structures.

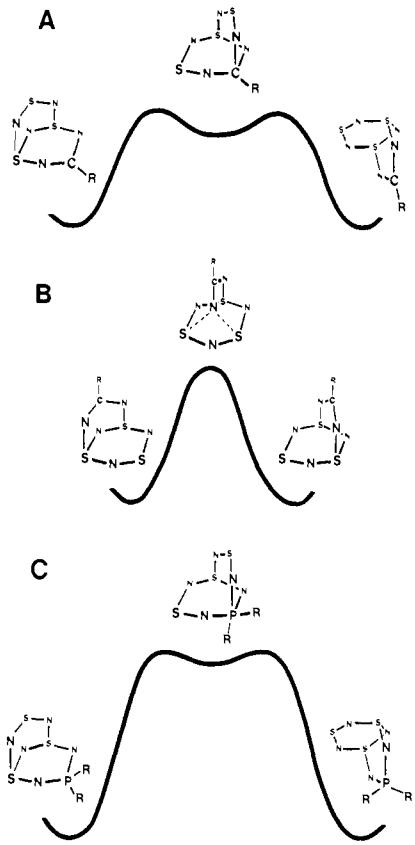

Figure 3. Qualitative internal energy profiles for 1,3-shifts via carbon (A) and sulfur (B) in **1** and via phosphorus (C) in **6**.

The slow rate of scrambling in **6** can be understood in terms of the probable transition state for the migration of an NSN bridge to phosphorus (Figure 3C).[18] While the S_a–N_b bonds in $H_2PN_5S_3$ are relatively free to migrate (see Table III), the shift is impeded by the need to traverse a high-energy structure possessing a five-coordinate phosphorus atom.[17] While such a geometry is not uncommon for phosphorus, its stability is well known to be dependent on the electronegativity of the ligand field. The proposed intermediate for the phosphorus pathway would involve a $R_2P(N{=})_3$ structure, an unstable ligand environment for hypervalent phosphorus.[19]

While the rate of scrambling via carbon in **1** is much faster than via phosphorus in **6**, the rate of NSN elimination from **1** is much slower than from **6**. Indeed, **1** can be sublimed in vacuo at 80 °C without decomposition. Moreover, although **1** does slowly degrade in boiling acetonitrile, the corresponding dithiatriazine **8** (Scheme V) is not produced: the isolated products are S_4N_4 and benzonitrile. This reversal in the rates of the 1,3-shift in, and

(14) Oakley, R. T. *Prog. Inorg. Chem.* **1988**, *36*, 299.
(15) Chivers, T.; Laidlaw, W. G.; Oakley, R. T.; Trsic, M. *J. Am. Chem. Soc.* **1980**, *102*, 5573.
(16) Boerē, R. T.; Cordes, A. W.; Oakley, R. T. *J. Chem. Soc., Chem. Commun.* **1985**, 929.

(17) We refer to structures A and C (shown in Figure 3) as intermediates, but it is not inconceivable that they are transition states. It suffices to say that we have been unable to observe them by spectroscopic methods; if either has a finite existence at all, its steady-state concentration is very low.
(18) There is, of course, a sulfur pathway in $R_2PN_5S_3$ structures. If, however, the phosphorus pathway is inoperative, this other route cannot be probed by the isotopic methods developed here. The high bond orders found for the N_a–S_a bonds in $H_2PN_5S_3$ suggest that it would be a relatively slow process.
(19) It is worth noting that the first $R_2PN_5S_3$ isolated (with R = F) was initially assigned a structure with a five-coordinate phosphorus; see: Roesky, H. W.; Petersen, O. *Angew. Chem., Int. Ed. Engl.* **1973**, *12*, 415. Later X-ray work confirmed a four-coordinate phosphorus, as in **6**; see: Weiss, J.; Ruppert, I.; Appel, R. *Z. Anorg. Allg. Chem.* **1974**, *406*, 329.

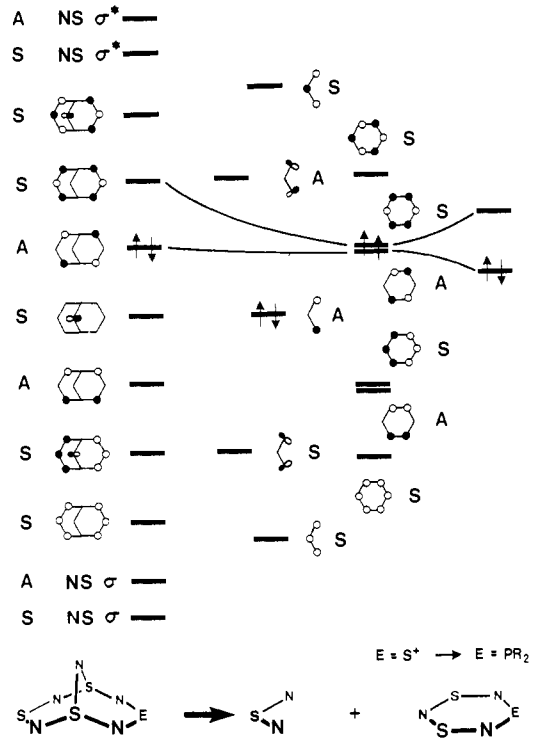

Figure 4. Qualitative orbital diagram illustrating the evolution of the MOs of a bicyclic EN_5S_3 molecule into those of a EN_3S_2 ring and a NSN fragment. The symbols S (symmetric) and A (antisymmetric) refer to orbital symmetries with respect to a mirror plane bisecting each molecule.

thermal elimination of NSN from, **1** and **6** can be readily understood with reference to Figure 4, which correlates the molecular orbitals of a generalized EN_5S_3 molecule as it cycloreverts into EN_3S_2 and NSN. When E = S^+, i.e., in $S_4N_5^+$ (**5**), the elimination of NSN (in its "90°" configuration)[20] yields the $S_3N_3^+$ cation, an 8π-system with a triplet ground state;[21] accordingly, this process should be symmetry forbidden. When S^+ is replaced by R_2P, the degeneracy of the uppermost orbitals of $S_3N_3^+$ is lifted, and the resulting $R_2PN_3S_2$ (**7**) is a stable singlet;[3] thermal elimination of NSN from the bicyclic structure **6** to yield **7** is therefore symmetry allowed.[12]

In the case of elimination of NSN from **1**, the symmetry-based classification is less clear-cut. The product of such a reaction, the dithiatriazine **8**, has been the subject of both experimental and theoretical interest. In a formal sense it is, like 7, an 8π-electron antiaromatic system. There are, to date, however, no structurally characterized examples of monomeric dithiatriazines; **8** itself exists as a cofacially bound dimer.[22] Recent ab initio molecular orbital and electron correlation calculations on model rings (RCN_3S_2, R = H, NH_2) related to **8** indicate that such species, although possessing singlet electronic ground states, have highly Jahn–Teller distorted (into C_s symmetry) structures.[23] The C_{2v} symmetry structure for HCN_3S_2, for example, lies some 14 kcal mol^{-1} above the C_s symmetry version. As a result of this predicted instability of the high-symmetry form of **8**, its generation by the concerted elimination of NSN from **1** is likely to be a relatively high-energy process. In a sense the cycloreversion is "almost" symmetry forbidden.

Reduction of $S_4N_5^+$ **5** to the corresponding anion $S_4N_5^-$ effects a major structural change. The two extra electrons occupy the LUMO of the cation (see Figure 4), a strongly antibonding π^*-type orbital distributed over the NSN wings. In response to the weakening of the local π-system, the structure folds into the more cage-like geometry (Scheme VII), with a close transannular S–S contact.[24] The reduction process should also lead to an inversion in the rates of thermal decomposition (loss of NSN) and skeletal scrambling. Although we have no kinetic data on the latter process, it is likely that, as Bartetzko and Gleiter pointed out,[6] the energy required to reopen the cage, that is, to break the S–S bond (Scheme VII), will inhibit the 1,3-shift pathway. Conversely, the thermal degradation of $S_4N_5^-$ to the aromatic 10π-electron $S_3N_3^-$ anion and NSN should be unrestricted by spin or orbital constraints (see Figure 4). Consistently, salts of $S_4N_5^-$ readily decompose via this route.[15]

Scheme VII

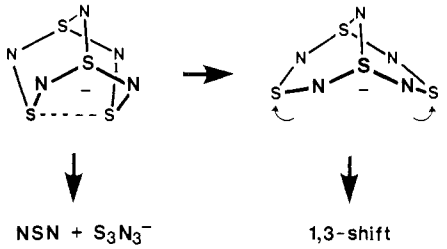

Table IV. Spin–Lattice Relaxation Times (s) in **1** (at 22 °C)

signal	δ^a	$T1^b$	$T1^c$
N1,2	330.1	9.1	1.5
N3,4	176.1	22.9	2.4
N5	54.9	27.2	3.4

[a] Referenced to NH_3(l) at 25 °C. [b] Solvent $CDCl_3$. [c] Solvent $CDCl_3$ with 0.05 M $Cr(acac)_3$.

Summary and Conclusion

The pseudodegenerate 1,3-shift reactions reported here suggest that the static picture of the molecular structures of sulfur–nitrogen systems, as revealed by X-ray studies, conceals a rich dynamic behavior. Additional theoretical and experimental studies to establish the generality of this concept, and its very practical relationship to the thermal instability of sulfur–nitrogen compounds, are in progress.

Experimental Section

Starting Materials and General Procedures. ^{15}N-labeled $PhCN_5S_3$ (**1**) was prepared by the slow addition of a solution of $PhC(NSiMe_3)N(SiMe_3)_2$[25] to a slurry of 99% ^{15}N-labeled $S_3N_3Cl_3$ in acetonitrile at 0 °C. The yellow crystalline precipitate was isolated by filtration as quickly as possible in order to prevent isotopic scrambling (sample purity was checked by infrared spectroscopy). The labeled $S_3N_3Cl_3$ was prepared as described previously[2] starting from 99% ^{15}N-labeled NH_4Cl (Mercke, Sharpe and Dohme). The large-scale preparation of $Ph_2PN_5S_3$ (**6**) from the reaction of $Ph_2P(NSiMe_3)N(SiMe_3)_2$ with $S_3N_3Cl_3$ has recently been reported.[11] In our work we used the same reaction (with 99% ^{15}N-labeled $S_3N_3Cl_3$), with toluene as solvent, but did not isolate the product. It was characterized by ^{31}P NMR (δ -21.0 with respect to external H_3PO_4; lit.[12] -21.3) and ^{15}N NMR (δ 322.0 (N1,2) and 79.2 (N5)), and then immediately thermolyzed in situ to $Ph_2PN_3S_2$ (**7**) by heating the toluene solution at reflux for 30 min. The product was purified by chromatography on Bio-Beads SX-8 before ^{15}N NMR analysis. The ^{15}N NMR spectrum of the isolated material showed a single doublet at δ 334.8 corresponding to nitrogen enrichment at the unique site.[8]

NMR Spectra and Kinetic Data Collection. NMR spectra were recorded on a Bruker WH-400 spectrometer using a broad-band 10-mm probe tuned to 40.5 MHz. ^{15}N chemical shifts (Table IV) were referenced to NH_3 (l) at 25 °C. Concern over potential errors in the use of signal intensities (i.e., peak integrations) as measures of ^{15}N concentration prompted us to determine the spin–lattice relaxation times $T1$ for the three signals in **1**. The inversion–recovery sequence method (π–τ–$\pi/2$) was employed for this purpose. A sweepwidth of 20 kHz and a $\pi/2$ pulse width of 100 μs were used for all peaks. Pulse delays were 120 s (for N1,2 and N3,4) and 180 s (for N5). The carrier frequency for each $T1$

(20) Laidlaw, W. G.; Trsic, M. *Inorg. Chem.* **1981**, *20*, 1792.
(21) Lau, W. M.; Westwood, N. P. C.; Palmer, M. H. *J. Am. Chem. Soc.* **1986**, *108*, 3229.
(22) Boerē, R. T.; French, C. L.; Oakley, R. T.; Cordes, A. W.; Privett, J. A. J.; Craig, S. L.; Graham, J. B. *J. Am. Chem. Soc.* **1985**, *107*, 7710.
(23) Hoffmeyer, R. E.; Chan, W.-T.; Goddard, J. D.; Oakley, R. T. *Can. J. Chem.* **1988**, *66*, 2279.
(24) Chivers, T.; Fielding, L.; Laidlaw, W. G.; Trsic, M. *Inorg. Chem.* **1979**, *18*, 3379.
(25) Boerē, R. T.; Reed, R. W.; Oakley, R. T. *J. Organomet. Chem.* **1987**, *331*, 161.

measurement was set 100 Hz upfield of the resonance being analyzed; τ-values ranged from 0.001 to 120 s, and good S/N ratios were achieved within 20-60 scans.

The long $T1$ values for **1** prohibited the rapid data collection needed to follow the scrambling process. In order to accelerate relaxation all kinetic NMR measurements were performed with a pulse width of 60 μs and with solutions 0.06 M **1** in $CDCl_3$ containing 0.05 M $Cr(acac)_3$ as a PARR. The presence of the PARR produced only very minor changes in chemical shifts and line widths, and allowed pulse delays to be reduced to 5 s. To ensure that differences in relaxation rates (see $T1$ values in Table IV were still not biasing the eigenintensities $Q1$ and $Q2$, the relative intensities of the three signals at $t = \infty$ were used to obtain numerical factors (ideally 2:2:1 for N1,2:N3,4:N5) needed for normalization of the kinetic data. S/N ratios of 60 were obtained within 250 or 450 scans. Over the temperature range 5-30 °C, the decay of $Q1$ and growth in $Q2$ could be reliably monitored for at least six half-lives, ie., 9.5 h at 5 °C and 2.0 h at 30 °C.

Molecular Orbital Calculations. MNDO calculations of charge densities and bond orders in EN_5S_3 structures were performed using the MOPAC suite of programs[26] operating on a SUN/3 workstation. The calculations were performed with full geometry optimization within a C_s symmetry constraint.

Acknowledgment. We thank the Natural Sciences and Engineering Research Council of Canada for financial support and an NSERC postdoctoral fellowship (to R.T.B.).

Appendix

Treatment of Kinetic Data. Combination of the two sets of coupled first-order processes shown in Scheme IV gives rise to the following secular determinant:[9]

$$\begin{vmatrix} -2(k_c+k_s)-\lambda & k_s & k_c & 0 & (k_c+k_s) \\ k_s & -2(k_c+k_s)-\lambda & 0 & k_c & (k_c+k_s) \\ k_c & 0 & -2(k_c+k_s)-\lambda & (k_c+2k_s) & 0 \\ 0 & k_c & (k_c+2k_s) & -2(k_c+k_s)-\lambda & 0 \\ (k_c+k_s) & (k_c+k_s) & 0 & 0 & -2(k_c+k_s)-\lambda \end{vmatrix} = 0$$

Solution of the above gives the eigenvalues:

$$\lambda_1 = -3k_s/2 - 5k_c/2 + (1/2)(5k_c^2 + 10k_ck_s + 9k_s2)^{1/2}$$

$$\lambda_2 = -7k_s/2 - 5k_c/2 + (1/2)(5k_c^2 + 2k_ck_s + k_s^2)^{1/2}$$

$$\lambda_3 = 0$$

$$\lambda_4 = -3k_s/2 - 5k_c/2 - (1/2)(5k_c^2 + 10k_ck_s + 9k_s^2)^{1/2}$$

$$\lambda_5 = -7k_s/2 - 5k_c/2 - (1/2)(5k_c^2 + 2k_ck_s + k_s^2)^{1/2}$$

The last three eigenvalues correspond to eigenintensities that are invariant with time. Numerical and algebraic solutions of the eigenvalue problem for λ_1 and λ_2 and the corresponding eigenintensities $Q1$ and $Q2$ were obtained using the program MAPLE operating on a SUN/3 workstation. Evaluation of the $t = \infty$ values of experimental intensities (including the $Q2$ eigenintensity) were performed with the program CONINFIN[27] (available through Project Seraphim). Linear regression analyses were carried out with Lotus 1-2-3.

Supplementary Material Available: Tables giving raw and normalized intensity versus time data, derivation of eigenintensities $Q1$ and $Q2$, first-order rate constants k_c and k_s, and Eyring analysis of rate constants k_c and k_s (8 pages). Ordering information is given on any masthead page.

(26) (a) Dewar, M. J. S.; Thiel, W. *J. Am. Chem. Soc.* **1977**, *99*, 4899. (b) *QCPE*, **1984**, No. 455 (MOPAC).

(27) Houser, J. J. *J. Chem. Educ.* **1982**, *59*, 776.

Oxygen-17 Nuclear Magnetic Resonance Spectroscopic Studies of Carbonmonoxy Hemoproteins

Hee Cheon Lee and Eric Oldfield*

Contribution from the School of Chemical Sciences, University of Illinois at Urbana-Champaign, 505 South Mathews Avenue, Urbana, Illinois 61801. *Received June 22, 1988*

Abstract: We have obtained surprisingly narrow ^{17}O nuclear magnetic resonance (NMR) spectra at 8.45 and 11.7 T (corresponding to ^{17}O frequencies of 48.8 and 67.8 MHz) from $C^{17}O$ ligands bound to aqueous ferrous myoglobin from *Physeter catodon* (sperm whale MbCO), from adult human ferrous hemoglobin (HbCO A), and from ferrous hemoglobin from *Oryctolagus cuniculus* (rabbit HbCO). The ^{17}O NMR signals from these hemoproteins are not only narrower than anticipated, but in the case of sperm whale MbCO the line shape is distinctly non-Lorentzian. We have thus used the dispersion versus absorption (DISPA) plot method to investigate the origin of these unusual line widths and line shapes and demonstrate that they originate from the multiexponential nature of quadrupolar relaxation outside of the "extreme-narrowing" limit ($\omega_0\tau_c > 1$). We find from the DISPA analysis and from spin-lattice relaxation time (T_1) measurements that the ^{17}O nuclear quadrupole coupling constant (QCC) for sperm whale MbCO is 0.95 MHz, and the rotational correlation time, τ_c, is 14 ns (at $\omega_0\tau_c = 5.8$). This indicates a rigid heme-CO unit in sperm whale MbCO. Applying the same type of analysis to human HbCO yields ^{17}O QCC values of 0.9 MHz and τ_c of 23 ns (at $\omega_0\tau_c = 10$). In all cases, our results are consistent with an ^{17}O chemical shift anisotropy ($\sigma_\parallel - \sigma_\perp$) value of about 800 ppm for the CO ligand. These results are important for several reasons: first, they represent the first observation of high-resolution ^{17}O NMR spectra of the CO ligands in metalloproteins. Second, they represent the first experimental demonstration of multiexponential relaxation of a spin $I = {}^5/_2$ nucleus and its complete analysis with relaxation theory. Third, our results on sperm whale MbCO, taken together with ^{13}C NMR relaxation data, indicate little "internal motion" of the heme-CO group in this system. Our results also demonstrate a linear relationship between the ^{17}O NMR chemical shift and ν_{CO}, the infrared stretching frequency of the CO ligand, and between the ^{17}O chemical shift and the CO binding affinity of the protein. In addition, the ^{17}O NMR results are also in good agreement with previous time-differential perturbed γ-ray angular correlation (PAC) results on [^{111}In]myglobin and -hemoglobin (Marshall, A. G.; Lee, K. M.; Martin, P. W. *J. Am. Chem. Soc.* **1980**, *102*, 1460), and some molecular interpretations of the NMR and PAC results are offered.

In the absence of functional interactions, when ligand binding sites may be assumed to be equivalent and independent, different hemoproteins show large differences in their affinity for, and rates of reaction with, the same ligand, even though the overall arrangements of the polypeptide chains are similar.[1] Available evidence implies that the reactivity of the heme in hemoproteins is primarily controlled by local effects due to neighboring groups

(1) Antonini, E.; Brunori, M. In *Hemoglobin and Myoglobin in Their Reactions with Ligands*; American Elsevier: New York, 1971.

0002-7863/89/1511-1584$01.50/0